Pilot point temperature regulation for thermal lesion control during ultrasound thermal therapy

H.-L. Liu[1] Y.-Y. Chen[1] J.-Y. Yen[2] W.-L. Lin[3]

[1]Department of Electrical Engineering, National Taiwan University, Taipei, Taiwan
[2]Department of Mechanical Engineering, National Taiwan University, Taipei, Taiwan
[3]Institute of Biomedical Engineering, National Taiwan University, Taipei, Taiwan

Abstract—*The fundamental goal of ultrasound thermal therapy is to provide proper thermal lesion formations for effective tumour treatment. The quality of the therapy depends mostly on its positional precision. To date, most ultrasound thermal therapy treatments have focused on the formation of power or temperature patterns. The non-linear and time-delay effects of thermal dose formation prohibit direct control of the thermal dose distribution. In the paper, the control of thermal lesions by regulation of the temperature of a pilot point is proposed. This scheme utilises the high correlation between temperature elevation and thermal dose at the forward boundary of thermal lesions. To verify the feasibility, a 2D ultrasound phased array system was used to generate thermal lesions of various sizes, and the temperature elevation required to generate a thermal dose threshold was investigated. Results showed that the required temperature elevation was found to be a reasonably constant value of 52.5°C under differing conditions when the focal area was small. When the focal area under consideration was large, the required temperature elevation became a monotonic function of blood perfusion rate, ranging from 49.2 to 52.5°C. When the reference temperature of the pilot point was set at a conservative value (52.5°C), the thermal lesions were controlled precisely under a wide range of blood perfusion and power pattern changes, tested by using a more realistic model that takes into account thermal-induced attenuation and blood perfusion changes. This changed the complex thermal dose control problem into a simple temperature regulation problem, which makes implementation of thermal lesion control easier, giving the scheme a high potential for application to current ultrasound thermal therapy systems.*

Keywords—*Pilot point temperature, Thermal lesion control, Ultrasound thermal therapy, 2D phased array*

Med. Biol. Eng. Comput., 2004, **42**, 178–188

1 Introduction

THE TECHNIQUE of ultrasound thermal therapy uses focused ultrasonic energy to ablate the tumour region while preventing damage to the surrounding normal tissue (TER HAAR, 1995; VISIOLI *et al.*, 1999; CHAN *et al.*, 2002). To achieve this, the boundary of the thermal lesions formed should be controlled to conform well to the target tumours.

To define the thermal lesion boundary effectively, one of the most widely accepted approaches is to use the concept of thermal dose (SAPARETO and DEWEY, 1984). In general, tissue that receives a thermal dose value over a certain threshold can be considered to be completely necrosed, and this has been verified through several experimental reports (DAMIANOU *et al.*, 1995; MCDANNOLD *et al.*, 2000). Therefore the thermal lesion determination problem can be transformed into a thermal dose control problem.

Controlling the thermal dose is difficult owing to the following two problems. First, the accumulation of thermal dose is a function of temperature and time and is highly non-linear (SAPARETO and DEWEY, 1984). Secondly, after the heating power is turned off, the thermal dose keeps accumulating, and this accumulation depends on different positions, blood perfusion rates and heating strategies (LIN *et al.*, 2001). For these two reasons, previous studies only focused on the issues of off-line optimisation of the thermal lesion formation (HUTCHINSON and HYNYNEN, 1996; DAUM and HYNYNEN, 1999; WAN *et al.*, 1999; LIU *et al.*, 2003). These optimised results could exhibit a substantial error compared with the actual results owing to improper assignment of tissue parameters or temperature-dependent property change (Daum and Hynynen showed that even using identical power and heating time can induce thermal lesions with 100% volume change in their experiments (DAUM and HYNYNEN, 1999)).

Correspondence should be addressed to Professor Yung-Yaw Chen; email: yychen@cc.ee.ntu.edu.tw

Paper received 26 February 2003 and in final form 4 November 2003
MBEC online number: 20043855

ARORA *et al.* (2002) proposed a model predictive control structure to attempt to achieve on-line control of the thermal dose at a single point. However, they only showed the results for a simplified 1D thermal model and neglected the 3D thermal conduction effect. The large amount of computation with this approach is another potential problem in implementation of this scheme into a real 3D problem.

Besides observing the input power to alter the thermal lesion, an alternative is to explore the relationship between the thermal lesion boundary and the required temperature elevation. One of the advantages is that the complex dynamics, including those from power to temperature, and then to thermal dose, can be reduced to simply dynamics from temperature to thermal dose. Moreover, the temperature is easily acquired and monitored. GRAHAM *et al.* (1999) proposed a similar idea that attempted to quantify the tissue damage using the temperature information from an MR thermal-sensitive image. Their study showed that, using a spherical transducer as the heating source, the thermal coagulation could be detected by observing the temperature within a 1 mm square spatial region. This strongly supports the belief that the preceding conclusion is still valid when different power patterns are generated using other heating transducers (for example, a 2D phased array system that can generate multiple foci to alter the focal region with different sizes), and has potential to control the thermal lesions by regulating the elevated temperature.

The purpose of this study was to quantify the temperature required to form the thermal lesion boundary in the sense of reaching the thermal dose threshold at the forward lesion boundary, and also to examine the feasibility of controlling the thermal lesion dimension by using temperature regulation. A 2D ultrasound phased array system was used to generate power depositions to form different sizes of thermal lesion.

First, the temperature required at the front boundary of tumours to achieve the thermal dose threshold was investigated using the linear thermal model, without consideration of temperature-dependent changes of parameters. Some important factors that affect this temperature level were analysed, including the thermal lesion size, thermal conduction, blood perfusion rate and the heating rate. Then, based on this analysis, a complete procedure to control the thermal lesion boundary was proposed. A non-linear thermal model considering the temperature-dependent attenuation, absorption and blood perfusion effects was used in this part. Some examples are provided to illustrate the accuracy and limitation of this scheme.

2 Method

2.1 *Ultrasound field calculation*

To calculate the ultrasonic pressure field, the transducer was modelled as a grid of point sources. Then, the Rayleigh–Sommerfeld integral was used to sum up the contribution of each point source r' to the point of the field at r (O'NEIL, 1949). The integral is given as

$$P(x, y, z) = \frac{i\rho ck}{2\pi} \int_s \frac{ue^{-(\alpha+ik)\cdot(r-r')}}{r-r'} dS \quad (1)$$

where ρ = tissue density (1050 kg m^{-3}), c = the speed of sound (1500 m s^{-1}), k = the wave number ($2\pi/\lambda$, where λ is the wavelength), u = the complex surface velocity of the source, and α = attenuation (constant value of 4.1 Np m^{-1} MHz^{-1} after the curved boundary at $z = 4$ cm, unless otherwise mentioned). In an attenuating medium, the absorbed power density q is given as (NYBORG, 1981)

$$q = 2\alpha I \quad (2)$$

with

$$I = \frac{P^2}{2\rho c}$$

where $I(x, y, z)$ is the intensity of the field. The computations of the acoustic pressure and the resulting absorbed power deposition were performed with a source grid size of $\lambda/6$. To simplify the calculation, the non-linear, refraction and scattering effects of wave propagation were not included.

2.2 *Power pattern generation by 2D ultrasound phased array*

To test the feasibility of the proposed strategy, a 2D ultrasound phased array was used, as shown in Fig. 1. The array, containing 400 spherically sectioned elements (20×20), is capable of generating foci 2 cm off the centre with sufficiently small side lobes (FAN and HYNYNEN, 1996). The driving frequency, diameter and radius of curvature were 1 MHz, 15 cm and 12 cm, respectively.

As the cross-sectional diameter of single foci is small (only 0.1–0.2 cm in diameter), a pseudo-inverse method and temporal switching technique were utilised to generate a large focal area. First, a multiple-foci power pattern was synthesised by actuating the elements with designed amplitude and phase signals using the pseudo-inverse method (EBBINI and CAIN, 1989). Secondly, several multiple-foci power patterns were designed to steer the foci to different locations at the focal depth. Then, these multiple-foci power patterns were sequentially actuated in a circular pattern to scan the focal area at the focal depth (DAUM and HYNYNEN, 1998).

The selected multiple-foci power pattern in our study was based on the design of Daum and Hynynen and is shown in Fig. 1, where the only difference is the restriction of the simultaneous foci number to four (compared with eight). The focal spacing in a single power pattern was at least 0.4 cm, which is suggested by FAN and HYNYNEN (1996) to reduce the constructive interference in the near field. The switching frequency between successive power patterns was set to be 20 Hz in this study and was fast enough to reduce the temperature fluctuation during scanning (DAUM and HYNYNEN, 1999).

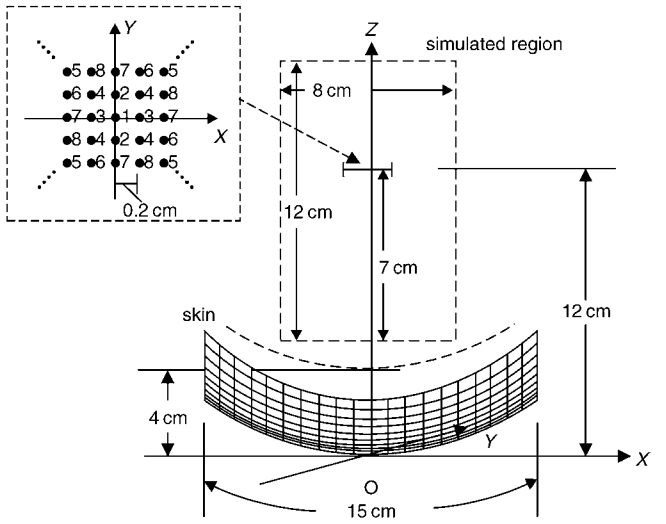

Fig. 1 *Geometry of 2D ultrasound phased array. Array is used to generate power patterns with various focal areas at focal depth $z = 12$ cm by temporally switching multiple-foci power patterns. Numbers in inset denote scanning sequence for generating multiple-foci power patterns and respective focal positions*

The focal area was selected as a squared region located at $z = 12$ cm, the size of which ranged from 0.4×0.4 to 2×2 cm^2 with a 0.4 cm increment. After cyclically driving the multiple-foci power patterns, the focal area could be scanned by foci with a 0.2 cm focal spacing, which is enough to provide sufficient thermal dose accumulation between foci (DAMIANOU and HYNYNEN, 1993).

2.3 *Temperature and thermal dose calculation*

The tissue temperature response T was calculated using the well-known bio-heat transfer equation (PENNES, 1948)

$$\rho c_t \frac{\partial T}{\partial t} = k\nabla^2 T - w_b c_b (T - T_{ar}) + q \tag{3}$$

where c_t and c_b are the specific heats of tissue and blood (both set to be 3770 J kg^{-1}°C^{-1}), k is the thermal conductivity of tissue (0.56 W m^{-1}°C^{-1}), w_b is the blood perfusion rate, and T_{ar} is the arterial blood temperature (37°C). This equation was solved using a numerical finite difference method (KOLIOS *et al.*, 1995), with all boundary and initial conditions set to 37°C. The time step and the grid spacing in the x-, y- and z-directions were 50 ms, 0.5 mm, 0.5 mm and 1 mm, respectively.

The thermal dose TD, in terms of equivalent minutes at 43°C, was used to estimate the necrosed tissue volume and was calculated using the following equation (DEWEY, 1994; PEARCE and THOMSEN, 1995; SAPARETO and DEWEY, 1984)

$$TD = \int_{t_0}^{t_f} R^{(T-43)} dt \approx \sum_{t_0}^{t_f} R^{(T-43)} \Delta t \tag{4}$$

where $R = 2$ for $T \geq 43$°C, $R = 4$ for 37°C $< T < 43$°C, Δt is the time step, and t_0 and t_f represent the initial and the final times, respectively. The TD value required for total necrosis ranges from 25 to 240 min for brain and muscle tissues, respectively (DAMIANOU *et al.*, 1995; DEWEY, 1994). In this study, a value of $TD = 240$ min was chosen as the threshold for complete heating.

2.4 *Temperature required to reach thermal dose threshold and its application in thermal lesion control*

To investigate the feasibility of controlling the thermal lesion using temperature information, the temperature elevation required to reach the thermal dose threshold was systematically analysed first. A 2D phased array was used to generate power patterns of various focal areas. We focused the analysis on the pilot point position of the lesion, which is defined as the front boundary of the lesion, along the central z-axis. The reason was that the extension of the thermal lesion in the skin direction exhibits large variations when different levels of power are applied (FAN and HYNYNEN, 1996). Moreover, monitoring the extension of thermal damage towards the skin to avoid the 'near field heating' problem is an important issue for external ultrasonic heating (FAN and HYNYNEN, 1996; LIU *et al.*, 2003). Possible factors affecting the required temperature include thermal lesion sizes, thermal conduction, blood perfusion rates and heating rates (high power–short duration or low power–long duration), and a complete analysis is given in Section 3.2.

The required temperature level quantified in the preceding analysis was used to control the thermal lesion dimension. The overall control procedure included three steps. The first step was to set a pilot point at the front boundary of the target tumour along the central z-axis. The second step was to select a suitable power deposition, with the focal area large enough to cover the cross-sectional area of the target tumour, by using the power synthesis method introduced in Section 2.3. The third step was to heat the tumour by delivering the selected power deposition with the maximum allowable power, until the temperature elevation of the pilot point reached the set level.

To demonstrate the control effect with consideration of non-linear thermal property change, the attenuation, absorption and blood perfusion rate were designated to be thermal dose-dependent. The change of the attenuation as a function of thermal dose was modelled according to KOLIOS *et al.* (1999), based on the experimental data of DAMIANOU *et al.* (1995)

$$\alpha(x, y, z) = \begin{cases} \alpha_1 \\ \alpha_1 + (\alpha_2 - \alpha_1) \cdot \dfrac{\log_{10}(TD) - 2}{7 - 2}, \\ \alpha_2 \end{cases} \begin{array}{l} \log_{10}(TD(x, y, z)) \leq 2 \\ 2 < \log_{10}(TD(x, y, z)) \leq 7 \\ \log_{10}(TD(x, y, z)) > 7 \end{array} \tag{5}$$

where $\alpha_1 = 4.1$ and $\alpha_2 = 9$ Np m^{-1} MHz^{-1}. The ultrasonic absorption was assumed to be 90% of the attenuation value (GERTNER *et al.*, 1997) throughout the entire temperature range. On the other hand, the blood perfusion rate was set to be a simple monotonic decrease with thermal dose, according to KOLIOS *et al.* (1999)

$$w(x, y, z) = \begin{cases} w_{b0} \\ w_{b0} \cdot \left(1 - \dfrac{\log_{10}(TD(x, y, z)) - 1}{2.5 - 1}\right) \\ 0 \end{cases} \begin{array}{l} \log_{10}(TD(x, y, z)) \leq 1 \\ 1 < \log_{10}(TD(x, y, z)) \leq 2.5 \\ \log_{10}(TD(x, y, z)) > 2.5 \end{array} \tag{6}$$

where w_{b0} is the initial blood perfusion rate. To solve (3) with consideration of non-linear tissue attenuation, absorption and blood perfusion change, the method described in PATANKAR (1980) was used. The free-field beam intensity was assumed not to be significantly distorted, and the attenuated beam could be calculated by integration of the attenuation coefficient over the axial distance traversed. The time and spatial grid were set to be identical to the above constant absorption and blood-perfusion cases, rather than the grid size being changed to accelerate the calculation used in KOLIOS *et al.* (1999).

3 Results

3.1 *Verification of the accuracy of the theoretical model*

To verify the accuracy of the ultrasound thermal model, we compared our theoretical model with published experimental and simulated data for a 2D phased array system (DAUM and HYNYNEN, 1999). Their 2D ultrasound phased array contains 256 elements with a driving frequency of 1.1 MHz. The diameter and the radius of curvature are 12 cm and 10 cm, respectively. The focal area produced in porcine thigh muscle is 1×1 cm^2 (containing 24 totally temporally switched, scanned foci), and the focal depth is about 5 cm beneath the skin.

Here, we repeated the same case using our theoretical model under the same conditions and compared the spatial distribution and the time response of the temperature with the reported experimental results. Figs 2*a* and *b* compare the measured and simulated temperature distributions at the end of sonication ($t = 20$ s), and Figs 2*c* and *d* compare the temperature responses at the focal depth and the pre-focal area.

These Figures show that our simulation results were quite close to the published simulated data (maximum deviation <5°C in front of the focal depth and <2°C at the focal depth) and

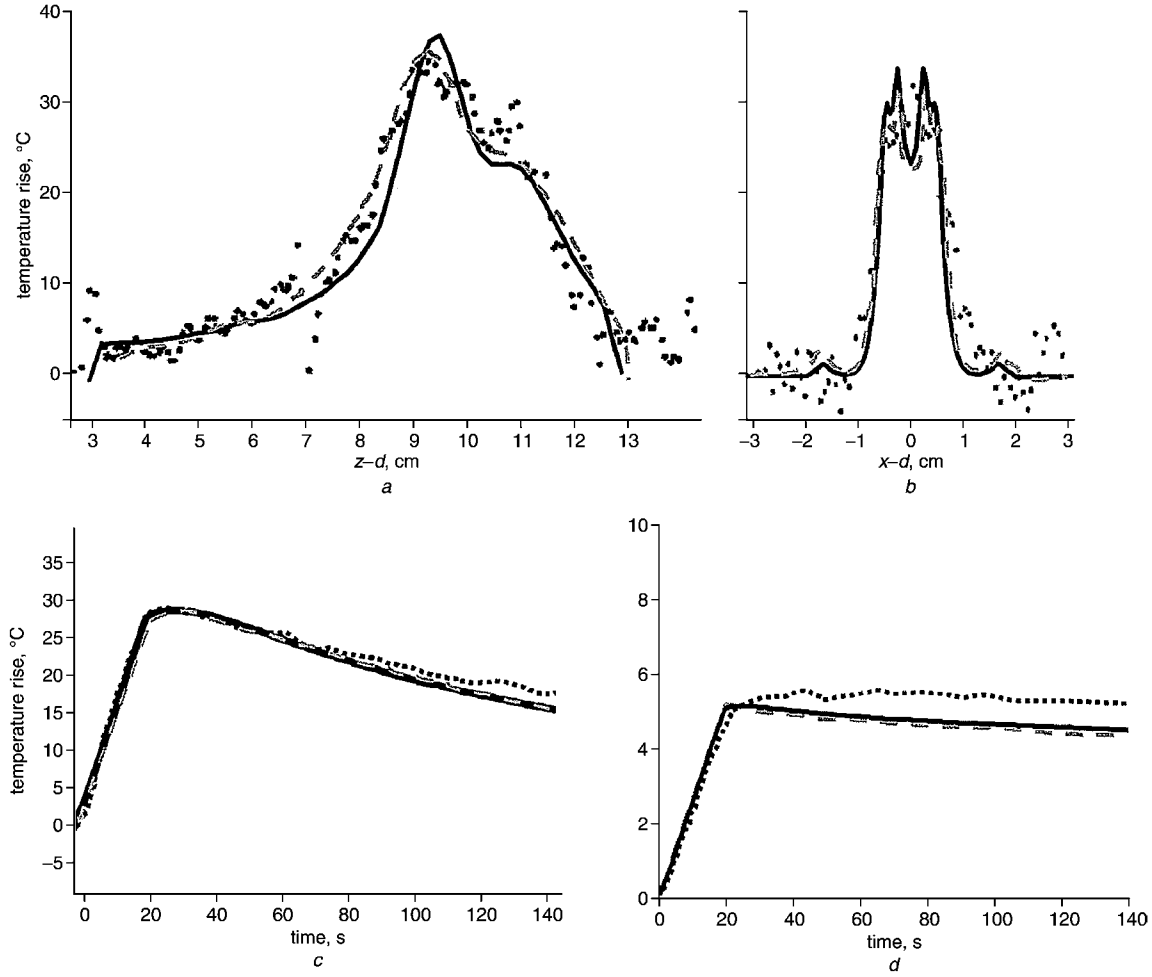

Fig. 2 *(—) Repeated simulated results compared with (. . . . .) experimental and (——) simulated data of 256-element 2D phased array system (DAUM and HYNYNEN, 1999). (a), (b) Spatial temperature distribution at end of sonication (20 s); temperature response (c) at focal depth and (d) at prefocal tissue (z = 6 cm); $w_b = 1$*

correlate well with the experimental data, both in spatial distribution and temporal response. In the temporal response, their reported and our simulated results both decay faster than the measured ones, especially in the pre-focal area shown in Fig. 2*d*. This can be caused by overestimation of the blood perfusion rate ($1\,kg\,m^{-3}\,s^{-1}$) in the simulation (DAUM and HYNYNEN, 1999).

3.2 *Analysis of temperature required to reach thermal dose threshold along power transmission direction*

Before use of the temperature regulation of the pilot point to control the thermal lesion boundary, the effects of various conditions should be analysed. These consist of different thermal lesion sizes, blood perfusion rates and heating rates. To perform this, we simply monitored the elevated temperature at the pilot point of thermal lesion under different conditions and then recorded the results.

3.2.1 *Effect of different thermal lesion sizes:* The first factor to be characterised was the thermal lesion size. Here, five power patterns were used, with focal areas from $0.4 \times 0.4\,cm^2$ to $2 \times 2\,cm^2$ generated by scanning 4–33 multiple foci patterns at a depth of $z = 12$ cm. Details of the settings are listed in Table 1. Fig. 3 shows the time-averaged absorbed power distributions of the five settings, defined as the sum of the scanned multiple-foci power distributions over the total power pattern number, and Fig. 4 shows the respective formed $TD = 240$ min regions with maximum temperatures of 65, 75 and 85°C under the blood perfusion rate of $0.5\,kg\,m^{-3}\,s^{-1}$ in the field.

Table 1 Five power patterns with different focal widths from 0.4 to 2 cm. Total foci number = total driven ultrasonic foci at 12 cm depth (multiple foci were driven simultaneously); total switched number = total switched number to drive overall ultrasonic foci; q_{max} = maximum absorbed power density of power pattern at focal depth. I_{max} = maximum instantaneous intensity at focal depth

Power patterns	A	B	C	D	E
Focal width, cm	0.4	0.8	1.2	1.6	2.0
Total foci number	9	25	49	81	121
Total switched number	4	8	15	25	33
q_{max}, W cm^{-3}	19.3	8.8	5.28	3.2	2.4
I_{max}, W cm^{-2}	1000	1000	1000	1000	1000

Fig. 5 shows three examples (power patterns A, C and E for reaching a maximum temperature of 75°C) of finding the temperatures required to reach $TD = 240$ min. The monitoring points were set at the front boundary of the lesion on the *z*-axis. Fig. 6 shows the required temperature as a function of focal width under different peak temperatures. Here, to consider the measured point position uncertainty in practical use, we observed the temperature needed to reach $TD = 240$ min at locations within a ± 0.2 cm shift off the central *z*-axis, and the bars in the figures represent the range of the variations. It shows that the temperature elevation decreases as the focal area of the power pattern increases (from 53.8 ± 2°C to 49.1 ± 0.2°C, with the focal area from 0.4×0.4 to $2 \times 2\,cm^2$). This is because the thermal conduction

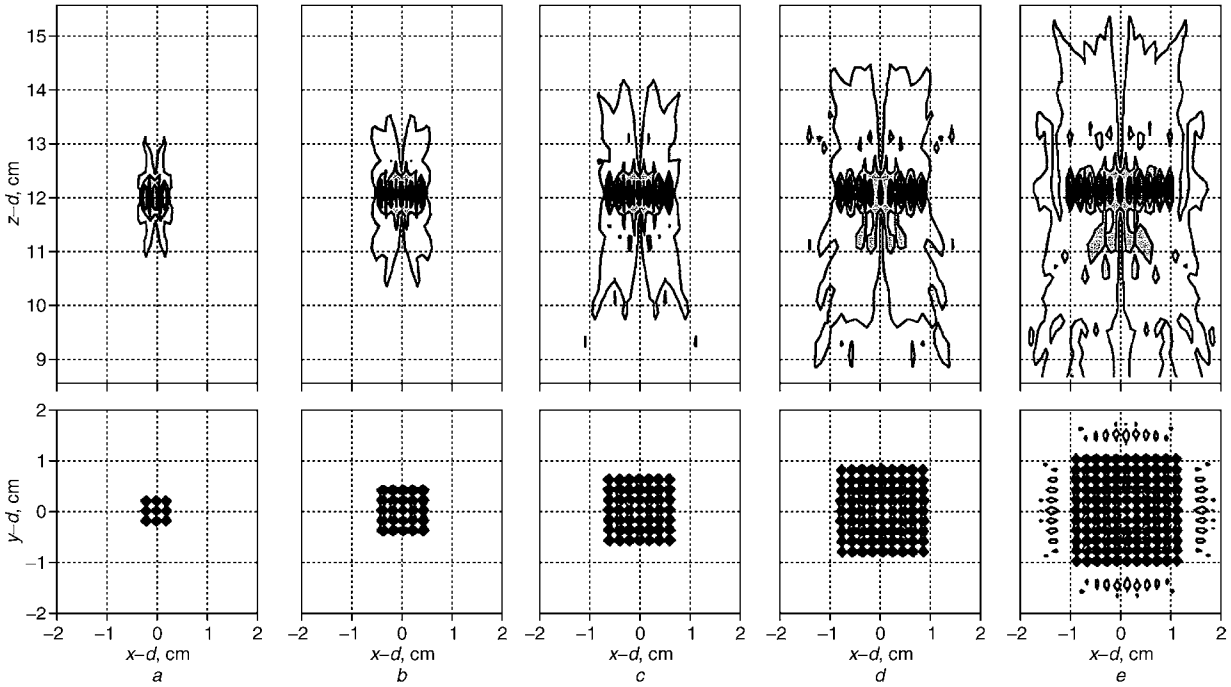

Fig. 3 *Averaged absorbed power depositions on x–z and x–y (z = 12 cm) planes with power patterns in Table 1. Contours are drawn at 20% intervals from 10 to 90%*

effect is relatively strong when the focal area is small and can dissipate energy quickly. It also implies that, to form a smaller thermal lesion, the regulated temperature at the forward boundary of lesions will be higher than that for a larger lesion.

Compared with the change in focal area, the effect of different heating durations was relatively small (within 2°C in most cases) and seems less critical. The influence of the measured position shift was also small in most cases in Fig. 6. The bending that occurred in the case of the 70°C maximum, as well as occasional crossing between curves may be caused by the positional uncertainty associated with each case, which can result in various indentations of the different power patterns.

3.2.2 *Effect of different blood perfusion rates:* The above results show that the temperature elevation at the target point can be changed under different thermal lesion sizes (especially changing the scanned focal area) owing to the various influences of the thermal conduction effect. Besides the thermal conduction effect, the blood perfusion change is another important factor. To investigate its influence, the value of the blood perfusion rate was changed from 0.5 to 10 $kg\,m^{-3}\,s^{-1}$ while the maximum temperature was kept at 80°C. The variation of the required temperature to reach $TD = 240$ min at the front boundary of the thermal lesions is shown in Fig. 7.

As the scanned focal area became small, the required temperature elevation was found to vary only slightly and remained high (53.8 ± 0.6°C for different blood perfusion rates). However, as the scanned focal area became large, the required temperatures became a monotonic function of the blood perfusion rate. This can be explained, in the case of a large focal area, by the thermal

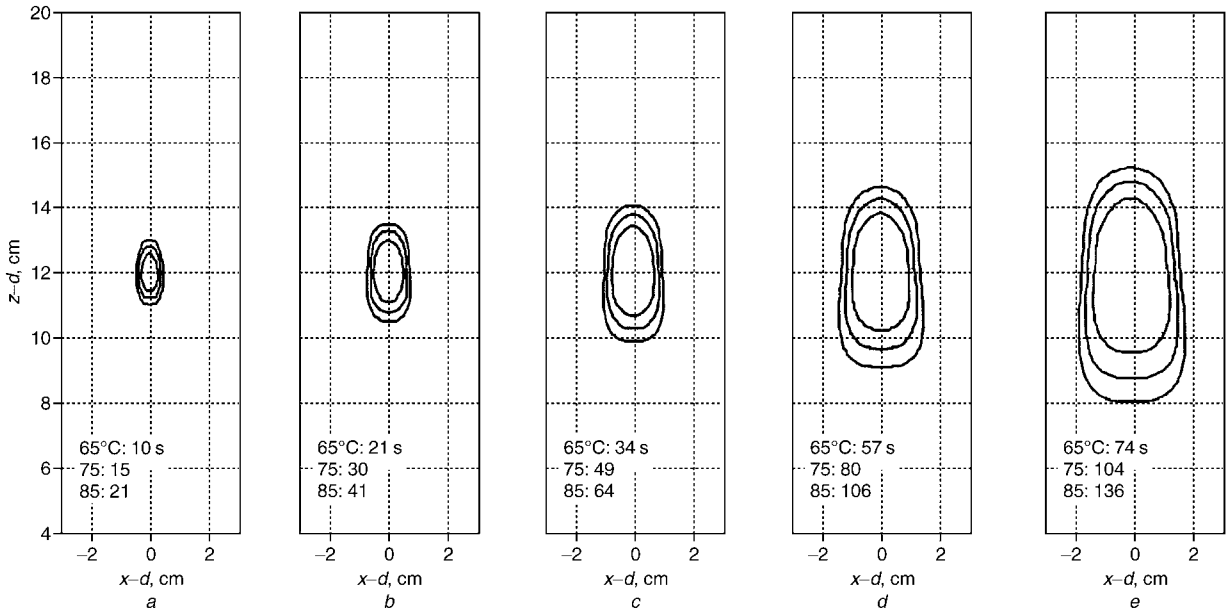

Fig. 4 *Regions of TD = 240 min generated by five power patterns in Table 1 while heating duration is altered to reach maximum temperatures of 65, 75 and 85°C*

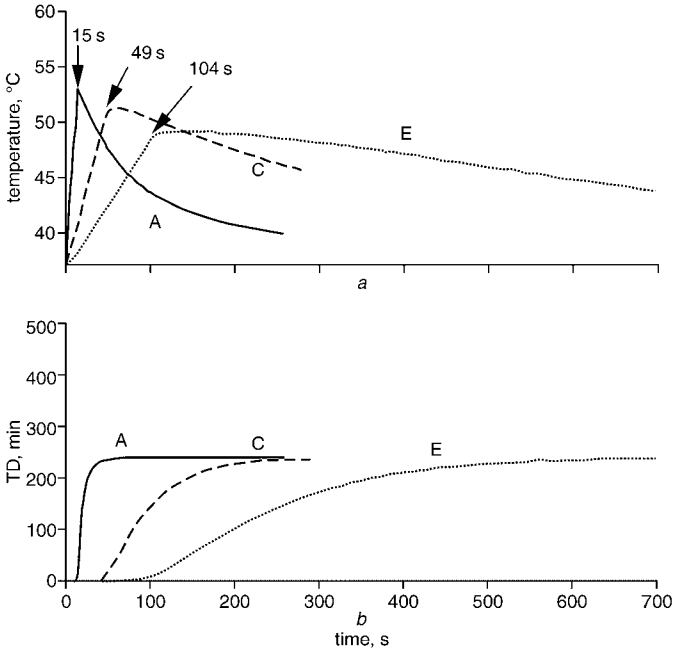

Fig. 5 *Temperature and thermal dose responses at front boundary of thermal lesions along z-axis. Power patterns A, C, E in Table 1 are used to reach maximum temperature of 75°C. Depth of monitoring points along central z-axis: A: z = 11.3 cm; C: z = 10.2 cm; E: z = 8.6 cm*

conduction not being very strong, so that the blood perfusion becomes the major factor affecting the temperature elevation. This observation is consistent with the conclusions in our previous works (LIN *et al.*, 2001; LIU *et al.*, 2003).

3.2.3 *Effect of different heating rates:* The above results show that the thermal conduction and the blood perfusion dominate the temperature required to reach $TD = 240$ min alternately, when the focal area is varied from small to large. However, the validity of this characteristic under different heating rates should be verified (for example, in a high-power, short-duration mode compared with a low-power, long-duration mode).

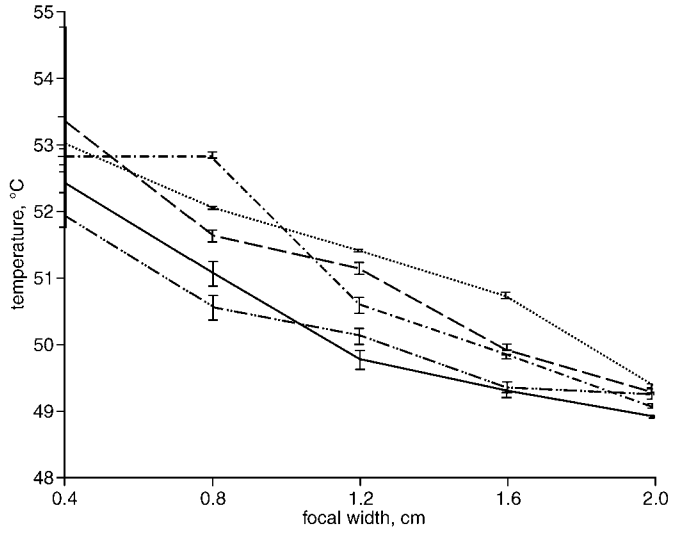

Fig. 6 *Temperature required to reach TD = 240 min at front boundary of thermal lesion as function of focal area under different peak temperatures. Bars represent range of variation under measured position shift along x–y-direction (up to ± 0.2 cm). Maximum temperature = (. . . . .) 65°C; (– – –) 70°C; (– · –) 75°C; (– · · – · ·) 80°C; (—) 85°C. $w_b = 0.5\,kg\,m^{-3}\,s^{-1}$*

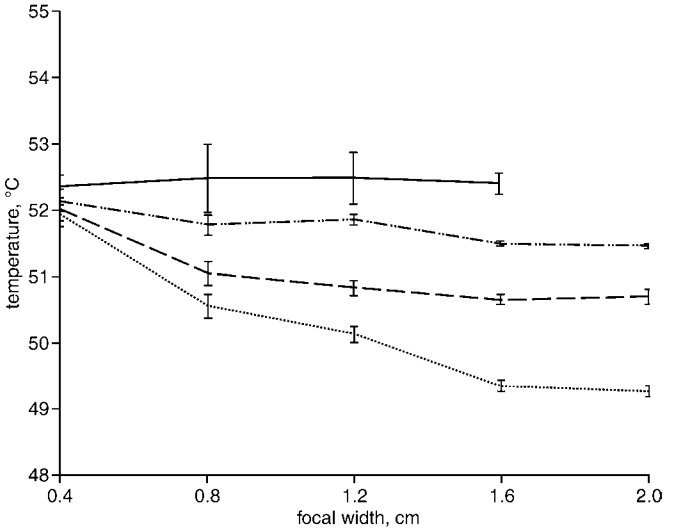

Fig. 7 *Temperatures required to reach TD = 240 min at front boundaries of thermal lesions as function of focal area under different blood perfusion rates from 0.5 to 10 $kg\,m^{-3}\,s^{-1}$. Bars represent range of variation under measured position shift along x–y-direction (up to ± 0.2 cm); $w_b = (. . . . .)$ 0.5 $kg\,m^{-3}\,s^{-1}$; (– – –) 2 $kg\,m^{-3}\,s^{-1}$; (– · · –) 5 $kg\,m^{-3}\,s^{-1}$; (—) 10 $kg\,m^{-3}\,s^{-1}$. Maximum temperature = 80°C*

To perform this test, absorbed power densities were varied from 2.4 to 19.2 W cm^{-3}, and heating durations were varied from 120 to 15 s, while the absorbed energy density was kept fixed without exceeding the threshold for transient cavitation (bubble expansion and violent collapse caused by high ultrasonic intensity, typically at a threshold of 1000 W cm^{-2} under the frequency used). Power patterns B and D were used to represent the power patterns of small and large scanned focal areas, respectively.

Results are shown in Figs 8*a* and *b*. In the results for pattern B, the thermal conduction effect is still the major factor, as the temperature elevation does not alter when the blood perfusion rate is varied. On the other hand, in the results for pattern D, the temperature elevation behaves as a monotonic function of the blood perfusion rate, showing that the blood perfusion is the major factor. The required temperature elevation is found to be nearly independent of different heating strategies, giving the same conclusion presented in Section 3.2.2.

3.3 *Control examples*

From the results of Figs 7 and 8, it can be observed that, for small lesions, the temperature required to achieve the thermal dose threshold in the case of a small focal area was about 52.5°C. In the large focal area case, the required temperature ranged from 49 to 52.5°C when the blood perfusion rate changed. Hence, to insure complete necrosis of the target tumours and to simplify the control procedure, the elevated temperature at the front boundary of the target region was controlled to reach 52.5°C.

In the following, we show the control results under two conditions. The first was for tumours that are of rectangular shape and similar to the thermal lesions of single exposure. The second was for tumours that are not rectangular in shape. In this part of the simulations, non-constancy of the thermal property was taken into account. The attenuation and absorption coefficients in the simulated field were varied according to the relationship of (5), and the blood perfusion rates in the field were also altered according to the relationship of (6).

3.3.1 *Tumours coverable by single thermal lesions:* In the first condition, three target tumours (all centred at $z = 12$ cm), with

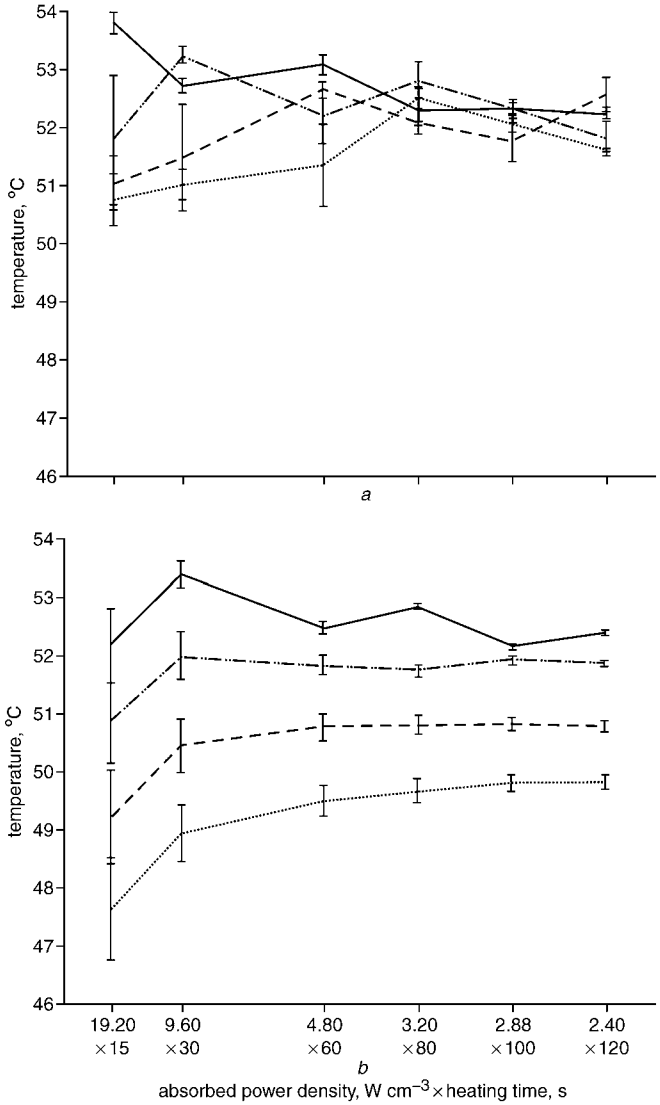

Fig. 8 *Temperatures required to reach TD = 240 min at front boundaries of thermal lesion as function of heating strategy (absorbed energy density fixed) under different blood perfusion rates while using (a) power pattern B and (b) power pattern D. Bars represent range of variation under measured position shift along x–y-direction (up to ± 0.2 cm); w_b = (. . . . .) 0.5 kg m^{-3} s^{-1}; (——) 2 kg m^{-3} s^{-1}; (– · –) 5 kg m^{-3} s^{-1}; (—) 10 kg m^{-3} s^{-1}*

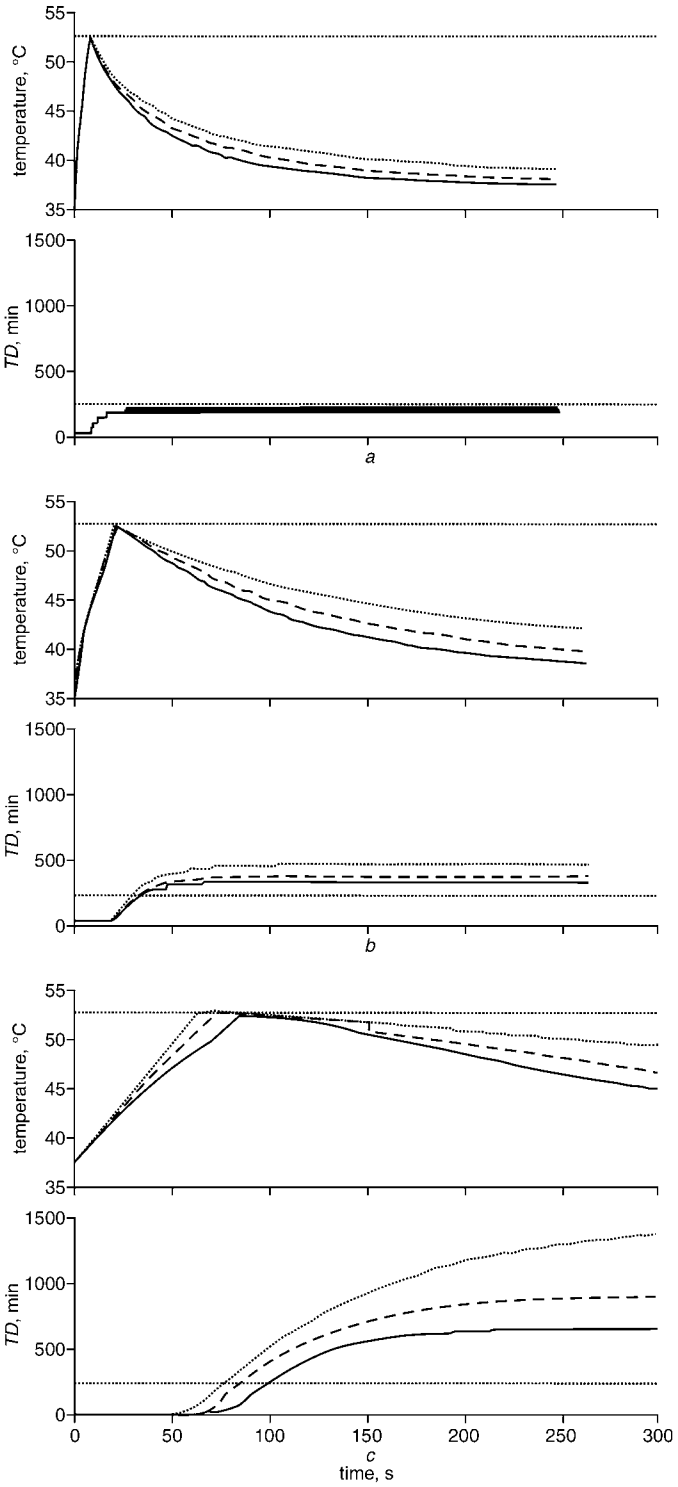

Fig. 9 *Temperature and thermal dose responses of designated pilot point (z = 11.5, 11 and 10 cm along z-axis) while power patterns (a) A, (b) B and (c) E are delivered under different w_{b0} = (. . . . .) 0.5, (– – –) 5 and (—) 10 kg m^{-3} s^{-1}. Controlled temperatures at designated pilot points for all cases are set to 52.5°C. A: z = 11.5 cm; B: z = 11 cm; E: z = 10 cm*

lengths of 1, 2 and 4 cm and widths of 0.5, 1 and 2 cm, respectively, were assumed to demonstrate the case that tumours can be covered by single thermal lesions. Meanwhile, different initial blood perfusion rates w_{b0} of 0.5, 5 and 10 kg m^{-3} s^{-1} were assigned.

To meet the cross-sectional areas of the designed target regions for these three cases, power patterns A, B and E were selected, according to the lesion estimation from Figs 3 and 4. The positions of the pilot points for these three cases were set to 11.5, 11 and 10 cm along the central z-axis. The regulated temperatures at these points were all set at 52.5°C. Fig. 9 shows the respective temperature and thermal dose responses at the set pilot points, and the resulting thermal dose distributions are shown in Fig. 10.

It can be seen that, if power pattern A is delivered, this scheme offers a precise thermal dose estimation to reach $TD = 240$ min. The temperature build-ups and decays are faster than in other cases and are also insensitive to different initial blood perfusion rates. The thermal lesions can be precisely controlled and indicated by the pilot point positions.

For the case of larger power patterns B and E, the temperature build-up and decay were relatively slow. The accumulated thermal dose values exceeded $TD = 240$ min and were more sensitive to blood perfusion rates, as shown in Fig. 10. However, the estimated position errors to reach $TD = 240$ min were still small and within 2 mm. An exception occurred in the large cross-sectional area case under a low blood perfusion rate (about 0.4 cm in front extension). This is because the regulated temperature of 52.5°C for pattern E was relatively higher than the required level (compared with 49°C), and the effect of blood

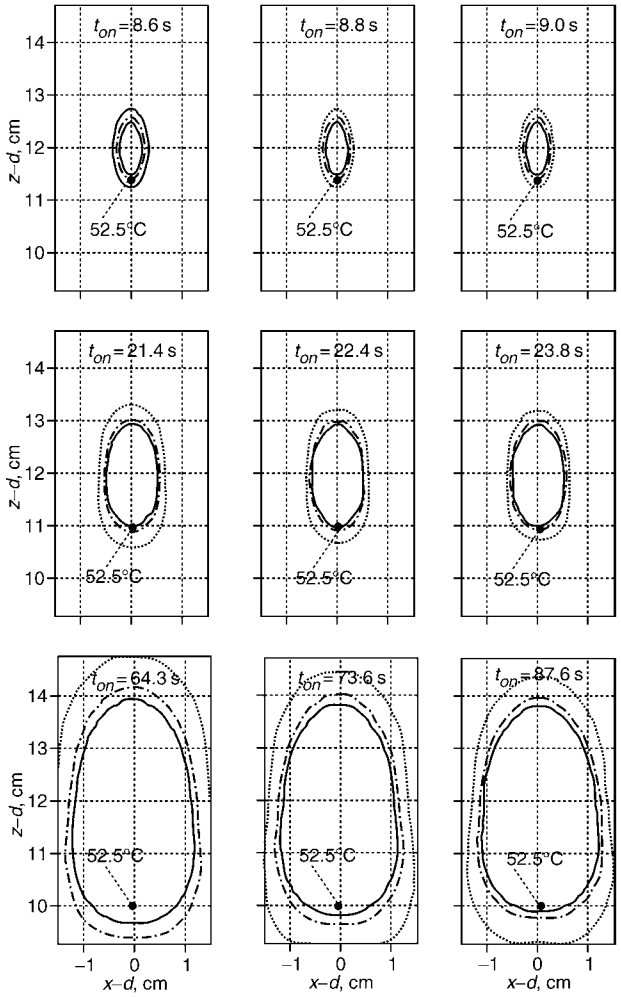

Fig. 10 *Thermal lesions generated with different power patterns (A, B and E) and different blood perfusion rates (0.5, 5 and 10 kg m^{-3} s^{-1}) by raising temperature of pilot points to reach 52.5°C. Contours show regions of thermal dose higher than 10, 100 and 240 min, and t_{on} represents exposure time*

perfusion is more apparent in larger thermal lesion cases according to the former analysis.

The maximum temperatures throughout the controlled cases were all below 80°C. The maximum attenuation of 9 Np m^{-1} MHz^{-1} and zero blood perfusion rates could be reached around the focal regions. Another observation from Fig. 10 is that the centre of the generated lesions shifts towards the skin apparently as the lesion extends.

3.3.2 *Tumours that cannot be covered by single thermal lesions:* The second condition was for tumours that cannot be covered by single thermal lesions. To perform this treatment, the target region can be divided into several smaller sub-regions and then heated sequentially. Here, two cubic regions of $2 \times 2 \times 2$ and $4 \times 4 \times 4$ cm^3, with centres at about $z = 12$ cm, were regarded as the target regions. These two regions were both divided into four sub-regions, each with volumes of $1 \times 1 \times 2$ and $2 \times 2 \times 4$ cm^3 (longer in the z-direction), respectively. The power patterns B and E in Table 1 were used to heat the sub-regions.

For each case, four pilot points were set to control the thermal lesion extension within each sub-region, and the regulated temperatures were all set to 52.5°C. To cover the target region as completely as possible, the pilot points were set 0.2 cm shallower than the target region boundary located on each sub-region's central axis. Between the heating of two different sub-regions, a cooling time interval was introduced to let the temperatures in the field all decay to below 43°C and prevent near-field overheating caused by thermal dose accumulation (LIN *et al.*, 2001).

The heating sequence of the four sub-regions, shown in Fig. 11, was designed to be able to dissipate the heat energy more easily and to shorten the introduced cooling time interval (LIN *et al.*, 2001). Fig. 11 shows the two generated thermal lesions, and the respective temperature and thermal dose responses of the pilot point are shown in Fig. 12. The generated lesions both conformed well to the target regions, and the forward lesion boundaries of both cases were both precisely controlled by these pilot points.

Fig. 12 shows that the temperature of each pilot point was raised to 52.5°C in sequence, and the cumulative thermal dose values of the four positions were identical. This means that the cooling period selected to decay the pilot-point temperature below 43°C can effectively avoid the thermal damage extension towards the skin.

4 Discussions

4.1 *Significance of this study*

In this study, the temperature level required to determine the thermal lesion boundary was quantified to satisfy most heating conditions, and this was also utilised to control the thermal lesion by regulating the temperature of a set pilot point. The thermal lesions could be precisely controlled in most cases. Moreover, compared with the comprehensive model prediction control method, this study offers a simple and easy-to-implement structure to provide closed-loop thermal lesion control.

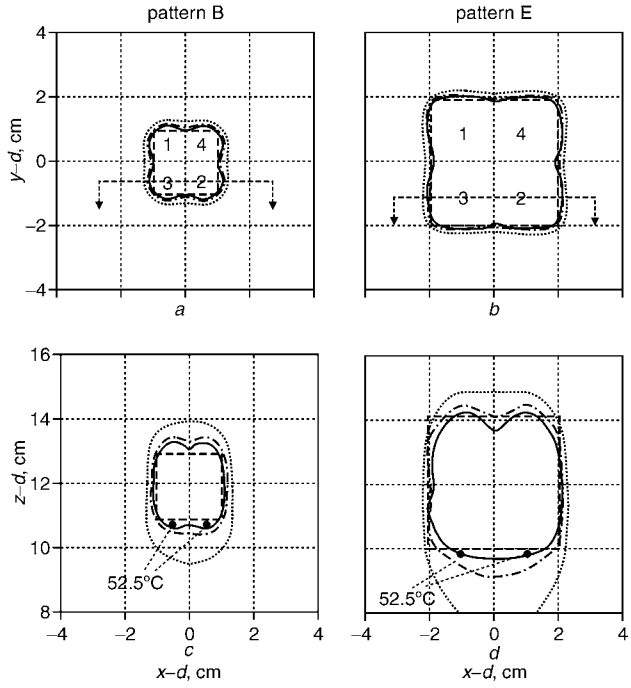

Fig. 11 *Two target regions of $2 \times 2 \times 2$ cm^3 and $4 \times 4 \times 4$ cm^3, divided into four sub-regions that are sequentially heated using power patterns B and E, respectively. (a), (b) thermal dose distribution on x–y plane at $z = 12$ cm; (c), (d) thermal dose distribution on x–z plane cut from broken lines in (a) and (b). Contours show regions of thermal dose higher than 10, 100 and 240 min*

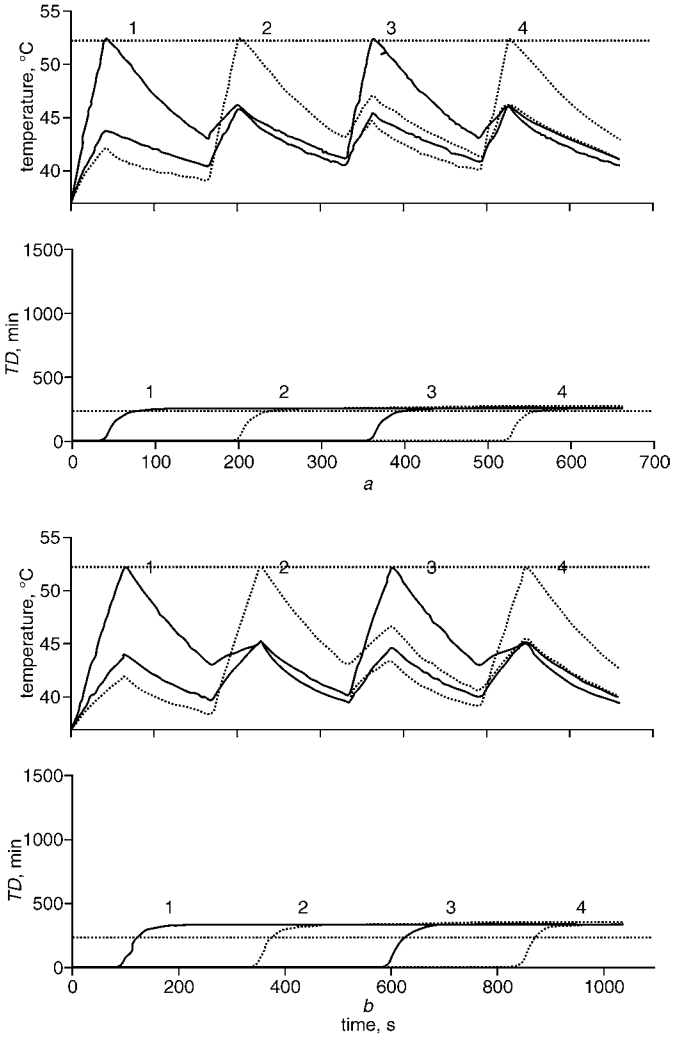

Fig. 12 *Temperature and thermal dose responses at designated pilot points, located at $z = 10.8$ cm and 9.8 cm, and ahead of each sub-region in case of $2 \times 2 \times 2$ and $4 \times 4 \times 4$ cm^3 treatment regions, respectively. Initial blood perfusion rates w_{b0} in both cases are set to 5 kg m^{-3} s^{-1}, and regulated temperatures are set to 52.5°C. (a) pattern B; (b) pattern E*

4.2 *Comparison with former studies of temperatures required to discriminate the lesion boundary*

Quantifying the critical temperature to form the thermal lesion boundary is important, as the necrosed region can be directly estimated through temperature monitoring rather than a comprehensive thermal dose prediction. This study shows that the required temperature to reach $TD = 240$ min is about 52.5°C for small focal area lesions (about 4 mm in width) and becomes a monotonic function of blood perfusion rate (ranging from 49 to 52.5°C for $w_b = 0.5$–10 kg m^{-3} s^{-1}, according to Fig. 8).

In the small lesion case, GRAHAM *et al.* (1999) used a spherical transducer to induce thermal lesions 3–4 mm wide and used an MR thermometry technique to perform temperature acquisition. The reported optimum discriminated temperatures for the necrosed region are about 53 ± 2°C and 54 ± 2°C in liver and kidney, respectively, which are very close to our proposed value in the small thermal lesion case.

For a larger thermal lesion case, DAUM and HYNYNEN (1999) showed that a 2D phased array can effectively induce a large thermal lesion over 1×1 cm^2 of cross-sectional area in porcine thigh muscle ($w_b = 0.5$–1 kg m^{-3} s^{-1}), which was verified both using the MR image and MR thermometry. The temperature required at the forward boundary of the lesion was found to be about 49–51°C after comparison with the thermal dose 240 min contours and the temperature distributions at the end of the heating session. This is also consistent with our observation.

On the other hand, ARORA *et al.* (2002) proposed a model predictive control structure to control the accumulated thermal dose reaching the hyperthermic level about $TD = 30$–40 min. From observation of their controlled cases, the temperature at the control point tends to be maintained at a consistent value of about 45°C for a period of about 10 min. To transfer this to reach our treatment requirement of 240 min within 0.5–1 min of the heating period for a small lesion, a rough estimation of temperature increment using (4) is about 6–7°C (i.e. 51–52°C). Although our heating scenario differs from their approach (on-and-off compared with the maintaining of a fixed temperature level), it still shows a similar conclusion to generate the required temperature level to determine the thermal lesion boundary.

4.3 *Changes of attenuation as a function of temperature*

In this study, to simplify the analysis of the temperature level required to reach the thermal dose threshold, a constant attenuation and blood perfusion model was used. Then, the temperature-dependent changes of the parameters were considered in the control examples to show the validity and effectiveness of the control scheme in more realistic conditions. Results showed that the thermal lesions can be still controlled precisely in most cases, according to the linear thermal model analysis.

A previous study shows that, at 65°C, the ultrasound attenuation coefficient has a 100% maximum increment in muscle tissue, and about a 90% increment in liver and kidney tissue (DAMIANOU *et al.*, 1997). However, it was also found that there is no attenuation increment until the heating temperature reaches 55°C, which is proposed in *ex vivo* muscle, kidney and liver tissues (DAMIANOU *et al.*, 1997; WORTHINGTON and SHERAR, 2001; GERNTER *et al.*, 1997). A reasonable explanation of the high control precision in the non-linear thermal model is that the regulated temperature at the pilot point is only 52.5°C and is not high enough to induce a noticeable attenuation change.

Even though there is little influence at the pilot point, it should be also noticed that the maximum temperature cannot reach the tissue boiling temperature of 100°C. The reason is that the bubble or cavity induced by the boiling effect would largely scatter and block the ultrasonic energy and may induce unexpected lesion formations, such as the significant 'lesion shifting effect' or 'tadpole-like lesions' (MEANEY *et al.*, 2000; CHEN *et al.*, 2003).

In our test, the maximum temperature evaluated with the non-linear thermal model was about 5–10°C higher than the value predicted by the linear thermal model, and the maximum temperatures in the field were all below 80°C and were still safe from tissue boiling. However, it was also found that the temperatures increase very fast when the assigned pilot-point position moves towards the skin to extend the lesion dimension. To avoid building up an unacceptable maximum temperature, the range of the pilot point position should be limited. For example, in our own tests, delivering pattern A and setting the pilot point from 0.5 to 1.5 cm (i.e. lesions of about 1–3 cm in length) were found to be satisfactory.

4.4 *Potential errors for this scheme and solutions*

The proposed thermal dose control scheme can be used to control precisely the thermal lesion boundary in most cases while using a fixed reference temperature level. However, in this scheme, there still exist controlled errors resulting from two causes: one is the simplified regulated temperature setting of 52.5°C, and the other is the temperature measuring error inherent in the thermometry system.

First, a simplified, regulated temperature of 52.5°C is suitable when treating a small region but could be slightly higher for a larger region, especially for a low blood perfusion condition. This results in an overestimation of the formed thermal lesion length. To solve this, the controlled temperature elevation can be altered to fit different blood perfusion rates, based on the results of Figs 7 and 8. This can provide a more accurate temperature elevation and forms more accurate lesions to conform to the target boundaries.

The influence of the temperature-measurement error is another concern. Nowadays, MR thermometry is a promising technique to measure temperature non-invasively. However, the reported temperature measurement error can be up to ± 3°C (GRAHAM *et al.*, 1999), and the sampling time for one image frame cannot be truly real time (4–7 s) (HYNYNEN *et al.*, 1999; 2003). This delay in temperature measurement may decrease the control precision significantly. One alternative is to use the thermocouple to perform the temperature acquisition. The advantage is that the precision is much higher than in MR thermometry (less than ± 0.2°C) (HYNYNEN and EDWARDS, 1989), and it is quite suitable for this proposed single point control structure. However, to avoid viscous heating by the thermocouple during heating, the heating power should be turned off (about a period of 2–3 s) (HYNYNEN and EDWARDS, 1989) during the measurement interval. The discontinuous nature of the monitored temperature response may also possibly decrease the precision of the control; however, some interpolation algorithms can be added to smooth out this acquired temperature response.

4.5 *Extension towards 3D thermal lesion volume estimation*

The proposed pilot point temperature regulation scheme is based on a simple temperature feedback to determine the thermal lesion dimensions. This offers a great advantage to reduce the temperature monitoring points and is easily implemented in invasive thermometry systems, for example, using thermocouples.

When this method is extended to control the entire thermal lesion volume, multiple temperature monitoring points should be set at the boundary of the target region, and the same temperature regulation scheme should be applied for each point. Among these monitoring positions, the ones along the cross-sectional direction and power transmission direction are both critical and should be monitored.

In our tests, the 52.5°C temperature contour could had a better determination at the forward and backward boundary, but had an overestimation along the cross-sectional direction. The reason is that the power gradient along the cross-sectional direction is rather higher than that along the power transmission direction. The thermal conduction, hence, takes away heat much faster, and a higher temperature to reach $TD = 240$ min is required (higher than the 54°C from our test).

In our previous study to optimise the power deposition during thermal therapy (LIN *et al.*, 2001), the ideal power pattern was set, which is uniformly distributed inside a cubic region with a sharp power gradient on the cubic boundary. The required temperature elevation for a 1 cm cubic case was found to be about 55°C, and this matches well with our observation here. Therefore to perform a 3D thermal lesion control, it seems a possible approach to set the regulated temperature along the power transmission direction to 52.5°C, while setting it to 55°C along the cross-sectional direction.

5 Conclusions

Pilot point temperature regulation for thermal lesion control in ultrasound thermal therapy is proposed in this paper. Compared with existing open-loop treatment planning, this strategy utilises the temperature feedback of a certain pilot point to provide closed-loop control on the formation of the thermal lesion. The simulation results show excellent control accuracy in lesion formation in most cases. The proposed method transforms the thermal dose control problem into a temperature regulation one, which is much easier to handle and will prove to be more effective in clinical treatments.

Acknowledgment—The authors would like to thank the National Science Council of Taiwan for partially supporting this research under contract NSC 90-2213-E-002-061.

References

ARORA, D., SKLIAR, M., and ROEMER, R. B. (2002): 'Model-predictive control of hyperthermia treatments', *IEEE Trans. Biomed. Eng.*, **49**, pp. 629–639

CHAN, A. H., FUJIMOTO, V. Y., MOORE, D. E., MARTIN, R. W., and VAEZY, S. (2002): 'An image-guided high intensity focused ultrasound device for uterine fibroids treatment', *Med. Phys.*, **29**, pp. 2611–2620

CLARKE, R. L., and TER HAAR, G. R. (1997): 'Temperature rise recorded during lesion formation by high-intensity focused ultrasound', *Ultrasound Med. Biol.*, **23**, pp. 299–306

DAMIANOU, C., and HYNYNEN, K. (1993): 'Focal spacing and near-field heating during pulsed high temperature ultrasound therapy', *Ultrasound Med. Biol.*, **19**, pp. 777–787

DAMIANOU, C. A., HYNYNEN, K., and FAN, X. (1995): 'Evaluation of accuray of a theoretical model for predicting the necrosed tissue volume during focused ultrasound surgery', *IEEE Trans. Ultrason. Ferroelect. Freq. Contr.*, **42**, pp. 182–187

DAMIANOU, C. A., SANGHVI, N. T., FRY, F. J., and MAASS-MORENO, R. (1997): 'Dependence of ultrasonic attenuation and absorption in dog soft tissues on temperature and thermal dose', *J. Acoust. Soc. Am.*, **102**, pp. 628–634

DAUM, D. R., and HYNYNEN, K. (1998): 'Thermal dose optimization via temporal switching in ultrasound surgery', *IEEE Trans. Ultrason. Ferroelec. Freq. Contr.*, **45**, pp. 208–215

DAUM, D. R., and HYNYNEN, K. (1999): 'A 256-element ultrasonic phased array system for the treatment of larger volumes of deep seated tissue', *IEEE Trans. Ultrason. Ferroelec. Freq. Contr.*, **46**, pp. 1254–1268

DEWEY, W. C. (1994): 'Arrhenius relationships from the molecules and cell to the clinic', *Int. J. Hyperthermia*, **10**, pp. 457–483

DUDAR, T., and JAIN, R. (1984): 'Differential response of normal and tumour microcirculation to hyperthermia', *Cancer Research*, **44**, pp. 605–612

EBBINI, E. S., and CAIN, C. A. (1989): 'Multiple-focus ultrasound phased-array pattern synthesis: optimal driving-signal distributions for hyperthermia', *IEEE Trans. Ultrason. Ferroelec. Freq. Contr.*, **36**, pp. 540–548

FAN, X., and HYNYNEN, K. (1996): 'Ultrasound surgery using multiple sonications - treatment time considerations', *Ultrasound Med. Biol.*, **22**, pp. 471–482

GERTENER, M. R., WILSON, B. C., and SHERAR, M. D. (1997): 'Ultrasound properties of liver tissue during heating', *Ultrasound Med. Biol.*, **23**, pp. 1395–1403

GRAHAM, S. J., CHEN, L., LEITCH, M., PETERS, R. D., BRONSKILL, M. J., FOSTER, F. S., HENKELMAN, R. M., and PLEWES, D. B. (1999): 'Quantifying tissue damage due to focused ultrasound heating observed by MRI', *Magn. Reson. Med.*, **41**, pp. 321–328

HUTCHINSON, E. B., and HYNYNEN, K. (1996): 'Intracavitary ultrasound phased arrays for noninvasive prostate surgery', *IEEE Trans. Ultrason. Ferroelect. Freq. Contr.*, **43**, pp. 1032–1042

HYNYNEN, K., and EDWARDS, D. K. (1989): 'Temperature measurements during ultrasound hyperthermia', *Med. Phys.*, **16**, pp. 618–626

HYNYNEN, K., MCDANNOLD, N., MARTIN, H., JOLESZ, F. A., and VYKHODTSEVA, N. (2003): 'The threshold for brain damage in rabbits induced by bursts of ultrasound in the presence of an ultrasound contrast agent', *Ultrasound Med. Biol.*, **29**, pp. 473–481

KOLIOS, M. C., SHERAR, M. D., and HUNT, J. W. (1995): 'Large vessel cooling in heated tissues: A numerical study', *Phys. Med. Biol.*, **40**, pp. 477–494
KOLIOS, M. C., SHERAR, M. D., and HUNT, J. W. (1999): 'Temperature dependent tissue properties and ultrasonic lesion formation', in SCOTT, E. (Ed.): *Advances in heat and mass transfer in biotechnology* (ASME, New York, 1999), pp. 113–118
LIN, W. L., LIANG, T. C., YEN, J. Y., LIU, H. L., and CHEN, Y. Y. (2001): 'Optimization of power deposition and a heating strategy for external ultrasound thermal therapy', *Med. Phys.*, **28**, pp. 2172–2181
LIU, H. L., CHEN, Y. Y., YEN, J. Y., and LIN, W. L. (2003): 'Treatment time reduction for large thermal lesions by using a multiple 1D ultrasound phased array system', *Phys. Med. Biol.*, **48**, pp. 1173–1190
MCDANNOLD, N. J., KING, R. L., JOLESZ, F. A., and HYNYNEN, K. (2000): 'Usefulness of MR imaging-derived thermometry and dosimetry in determining the threshold for tissue damage induced by thermal surgery in rabbits', *Radiology*, **216**, pp. 517–523
MEANEY, P. M., CAHILL, M. D., and TER HAAR, G. R. (2000): 'The intensity dependence of lesion position shift during focused ultrasound surgery', *Ultrasound Med. Biol.*, **26**, pp. 441–450
NYBORG, W. L. (1981): 'Heat generation by ultrasound in a relaxing medium', *J. Acoust. Soc. Amer.*, **1**, pp. 310–312
O'NEIL, H. T. (1949): 'Theory of focusing radiators', *J. Acoustic Soc. Am.*, **21**, pp. 516–526
PATANKAR, S. V. (1980): 'Numerical heat transfer and fluid flow' (Hemisphere, Washington, DC, 1980)
PEARCE, J., and THOMSEN, S. (1995): 'Rate process analysis of thermal damage', in WELCH, A. J., and VAN GEMERT, M. J. C. (Eds.): 'Optical-thermal response of laser-irradiated tissue' (Plenum, New York, 1995), pp. 561–606
PENNES, H. H. (1948): 'Analysis of tissue and arterial blood temperatures in the resting human forearm', *J. Appl. Phys.*, **1**, pp. 93–122
SAPARETO, S. A., and DEWEY, W. C. (1984): 'Thermal dose determination in cancer therapy', *Int. J. Radiat. Oncol. Biol. Phys.*, **10**, pp. 787–800
TER HAAR, G. R. (1995): 'Ultrasound focal beam surgery', *Ultrasound Med. Biol.*, **9**, pp. 1089–1100
VISIOLI, A., RIVENS, I., TER HAAR, G., HORWICH, A., HUDDART, R., MOSKOVIC, E., PADHANI, A., and GLEES, J. (1999): 'Preliminary results of a phase I dose escalation clinical trial using focused ultrasound in the treatment of localized tumours', *Eur. J. Ultrasound*, **9**, pp. 11–18
WAN, H., AARSVOLD, J., O'DONNELL, M., and CAIN, C. (1999): 'Thermal dose optimization for ultrasound tissue ablation', *IEEE Trans. Ultrason. Ferroelect. Freq. Contr.*, **46**, pp. 913–928
WORTHINGTON, A. E., and SHERAR, M. D. (2001): 'Changes in ultrasound properties of porcine kidney tissue during heating', *Ultrasound Med. Biol.*, **27**, pp. 673–682

Author's biography

HAO-LI LIU received the Bachelor degree in electrical engineering from the National Taipei University of Technology, Taipei, Taiwan in 1996, and the M.S. and PhD degrees in electrical engineering in 1998 and 2003, respectively, from National Taiwan University, Taipei. He is currently conducting research in ultrasound thermal therapy as an Assistant Adjunct Professor with the Department of Electronic Engineering, at the Tung-Nan Institute of Technology, Taipei, Taiwan.